Efficiency of randomised dynamic mode decomposition for reduced order modelling

D. A. Bistrian & I. M. Navon

Taylor & Francis
Taylor & Francis Group

Check for updates

Efficiency of randomised dynamic mode decomposition for reduced order modelling

D. A. Bistrian [a] and I. M. Navon [b]

[a]Department of Electrical Engineering and Industrial Informatics, Politehnica University of Timisoara, Hunedoara Romania;
[b]Department of Scientific Computing, Florida State University, Tallahassee, FL, USA

ABSTRACT

The purpose of this paper is the identification of a reduced order model (ROM) from numerical code output by non-intrusive techniques (i.e. not requiring projecting of the governing equations onto the reduced basis modes). In this paper, we perform a comparison between two methods of model order reduction based on dynamic mode decomposition (DMD). The first method is a deterministic (classic) DMD technique endowed with a dynamic filtering criterion of selection of modes used in the ROM model. The second method is an adaptive randomised DMD algorithm (ARDMD) based on a randomised singular value decomposition. This produced an accelerating algorithm, which is endowed with a few additional advantages. In addition, the reduced order model is guaranteed to satisfy the boundary conditions of the full model, which is crucial for surrogate modelling. For numerical illustration, we use the shallow water equations model.

1. Introduction

Identification of a reduced order model (ROM) from numerical or experimental data is a challenging topic in fluid dynamics. Many efforts were directed towards non-intrusive techniques, that do not require the projection of the governing equations onto the reduced basis modes, assuming that these governing equations or their numerical code are not known. The challenge among practitioners is a reliable approximation of the complex flow dynamics by models of low complexity, i.e. ROMs.

In the last decade, we have seen great advances of model order reduction techniques, like proper orthogonal decomposition (POD) (Du et al. 2013; Dimitriu, Stefanescu, and Navon 2015; Xiao et al. 2015; Stefanescu, Sandu, and Navon 2015; Towne, Schmidt, and Colonius 2018) and a promising technique rooted in Koopman mode theory (Koopman 1931), Koopman mode decomposition (KMD).

Koopman mode theory (Koopman 1931) introduced by the French-born American mathematician B. O. Koopman, provides a theoretical background for global modes analysis, hydrodynamic stability or triple decomposition in problems describing oscillating phenomena. The Croatian mathematician Mezic (2005) was the first to discover that normal modes of linear oscillations (which Mezic called *shape modes*) have their natural analogues – Koopman modes – in the context of non-linear dynamics. Koopman modes represent spatial flow structures which are associated with a single frequency. The time evolution of a mode is influenced by the multiplication of the complex eigenvalue of the Koopman operator weighted by the amplitude. Mezic (2005) was the first to apply the Koopman theory for the purposes of reduced order modelling. The advantage of the shape modes introduced by Mezic (2005) compared to POD modes is that each shape mode is associated with a pulsation, a growth rate and each mode has a single distinct frequency. Informative on the spectral properties of the Koopman operator are also the following references (Rowley et al. 2009, 2010; Chen, Tu, and Rowley 2012; Bagheri 2013; Mezic 2013).

A numerical algorithm to compute this type of modal decomposition was introduced by Schmid and Sesterhenn (2008) in 2008 and was called dynamic mode decomposition (DMD). This algorithm is classified as an Arnoldi-type method (Golub and Van Loan 1996) and is based on the theory of Krylov subspaces (Golub and Van Loan 1996).

Rowley et al. (2009) presented a technique for describing the global behaviour of complex non-linear flows. They have shown that the linearity assumption of the Koopman operator is not necessary.

Variants of DMD algorithm were used on a variety of examples ranging from fluid mechanics (Rowley et al. 2009; Frederich and Luchtenburg 2011; Schmid, Violato, and Scarano 2012; Balajewicz, Dowell, and Noack 2013), to non-linear dynamical systems and complex systems (Kutz et al. 2016), bifurcation analysis (Sayadi, Schmid, and Richecoeur 2015) and also to the niche fields like human–robot interaction (Berger et al. 2014) and neuroscience (Brunton et al. 2016).

So far we have noticed two directions in KMD technique, underlined in the three seminal papers on the topic, respectively, Mezic (2005), Rowley et al. (2009) and Schmid (2010). The straightforward approach is seeking a companion matrix employed to construct in the least squares sense the final data vector as a linear combination of all previous data vectors (Fiedler 2003; Rowley et al. 2009, 2010). Schmid (2010) explored the similarities between POD and DMD and recommended a more well-conditioned algorithm for DMD. In DMD the modes are not orthogonal, but one advantage of DMD compared to POD is that each DMD mode is associated with a pulsation, a growth rate and each mode has a single distinct frequency.

A considerable amount of work has focused on understanding and improving the method of DMD and several DMD procedures have been released: optimised DMD (Chen, Tu, and Rowley 2012), exact DMD (Tu et al. 2014), sparsity promoting DMD (Jovanovic, Schmid, and Nichols 2012), multi-resolution DMD (Kutz et al. 2015; Kutz, Fu, and Brunton 2016), extended DMD (Williams, Kevrekidis, and Rowley 2015), recursive DMD (Noack et al. 2015, 2016), DMD with control (Proctor, Brunton, and Kutz 2016), randomised DMD (Bistrian and Navon 2017b).

A comparative analysis of POD and DMD has been performed in the literature, to identify which of these decomposition techniques is more efficient for model order reduction (Muld, Efraimsson, and Henningson 2012; Semeraro, Bellani, and Lundell 2012; Towne, Schmidt, and Colonius 2018). These studies performed in various fields have demonstrated that POD and DMD are complementary methods contributing to the identification of the coherent structures.

A comparison of DMD vs. POD for model reduction was illustrated in our previous paper (Bistrian and Navon 2015), for the study of shallow water equations model. There are several major differences between these two decomposition methods. The spatial basis functions for DMD and POD respectively, offer an insight of the coherent structures in the flow field. The differences between POD and DMD occur due to the principles of their respective decomposition methods. The time evolution of a DMD mode is influenced by the multiplication of the complex eigenvalue of the Koopman operator weighted by the amplitude, while the time evolution of POD modes is described by the temporal coefficients. The POD modes are orthonormal in space with the energy inner product. In DMD, each mode oscillates at a single frequency, hence the expression that the DMD modes are orthogonal in time.

Selection of Koopman modes and amplitudes used for the flow reconstruction constitutes also the source of many discussions among modal decomposition practitioners (Tissot et al. 2014). For instance, a low-rank DMD algorithm was introduced in Jovanovic, Schmid, and Nichols (2012) to identify an a-priori specified number of modes that provide an optimal approximation of experimental or numerical snapshots at a certain time interval. Consequently, the modes and frequencies that have the strongest influence on the quality of approximation have been selected. Chen, Tu, and Rowley (2012) introduced an optimised DMD, which tailors the decomposition to a desired number of modes. This method minimises the total residual over all data vectors and uses simulated annealing and quasi-Newton minimisation iterative methods for selecting the frequencies. Several procedures for selecting the most influential modes in DMD can be found in our previous papers (Bistrian and Navon 2015; Alekseev et al. 2016; Bistrian and Navon 2017a) which we will discuss later.

The flow dynamics may be unpredictable. Neither the selection of the modes based on their amplitude, nor the selection based on the frequency, are certain to lead to the finding of the dominant modes, as was reported in Noack, Morzynski, and Tadmor (2011).

In the present work, we propose a comparison between two DMD algorithms. The first consists of a deterministic DMD method endowed with a vector filtering criterion to select the most influential modes. The second algorithm utilises an adaptive randomised DMD (ARDMD) to obtain a reduced basis in the offline stage, that does not require an additional selection algorithm of the DMD modes.

The remainder of the article is organised as follows. In Section 2 we recall the principles governing the DMD and we provide the description of the DMD algorithms employed for decomposition of numerical data. Sections 3 and 4 illustrate the impact of the above methods on the reduction of the shallow water equations model. Summary and conclusions are drawn in the final section.

2. Reduced order modelling based on DMD

2.1. The key steps of DMD

DMD is a data processing tool which is applied to numerical or experimental data, in order to identify the coherent structures of dynamics or for the purpose of surrogate modelling. In the present paper, we apply the method of DMD for an efficiently reduced-order modelling of numerical data. We outline in the following the key steps of DMD.

We proceed by collecting data $v_i(t, \mathbf{x}) = v(t_i, \mathbf{x})$, $t_i = i\Delta t$, $i = 0, \ldots, N$, at a constant sampling time Δt, $\mathbf{x}$ representing the spatial coordinates whether Cartesian or cylindrical. The two integer parameters N and M involved in the process of data acquisition have the following meanings:

$N + 1 = $ total number of snapshots taken in time, $M = $ number of spatial measurements per time snapshot.

We form a data matrix whose columns represent the individual data samples, called *the snapshot matrix*

$$V = [v_0 \quad v_1 \quad \cdots \quad v_N] \in \mathbb{R}^{M \times (N+1)}. \quad (1)$$

Each column v_i is a vector with M components, representing the numerical measurements. For simplicity of description, we consider here real data $v_i \in \mathbb{R}^M$.

The Koopman decomposition assumed that a propagator matrix $\mathcal{A}$ exists, that maps every vector column onto the next one

$$\{v_0, v_1 = \mathcal{A}v_0, v_2 = \mathcal{A}v_1 = \mathcal{A}^2 v_0, \ldots,$$
$$v_N = \mathcal{A}v_{N-1} = \mathcal{A}^N v_0\}. \quad (2)$$

The DMD algorithm constructs the best approximation of the propagator matrix $\mathcal{A}$. The next computational step consists in forming two data matrices from the snapshot sequence. A matrix V_0^{N-1} is formed with the first N columns and the matrix V_1^N contains the last N columns of V:

$$V_0^{N-1} = [v_0 \quad v_1 \quad \cdots \quad v_{N-1}] \in \mathbb{R}^{M \times N},$$
$$V_1^N = [v_1 \quad v_2 \quad \cdots \quad v_N] \in \mathbb{R}^{M \times N}. \quad (3)$$

For a sufficiently long sequence of the snapshots, we suppose that the last snapshot v_N can be written as a linear combination of previous N vectors, such that

$$v_N = c_0 v_0 + c_1 v_1 + \cdots + c_{N-1} v_{N-1} + \mathcal{R}, \quad (4)$$

in which $c_i \in \mathbb{R}, i = 0, \ldots, N - 1$ and $\mathcal{R}$ is the residual vector. We assemble the following relations:

$$\{v_1, v_2, \ldots, v_N\} = \mathcal{A}\{v_0, v_1, \ldots, v_{N-1}\}$$
$$= \{v_1, v_2, \ldots, V_0^{N-1} c\} + \mathcal{R}, \quad (5)$$

where $c = (c_0 \, c_1 \cdots c_{N-1})^{\mathrm{T}}$ is the unknown column vector.

In matrix notation form, Equation (5) reads

$$\mathcal{A}V_0^{N-1} = V_0^{N-1}\mathcal{S} + \mathcal{R}, \quad \mathcal{S} = \begin{pmatrix} 0 & \cdots & 0 & c_0 \\ 1 & & 0 & c_1 \\ \vdots & \vdots & \vdots & \vdots \\ 0 & \cdots & 1 & c_{N-1} \end{pmatrix}, \quad (6)$$

where $\mathcal{S}$ is the companion matrix.

Relation (6) is true when the residual

$$\mathcal{R} = v_N - V_0^{N-1} c \quad (7)$$

is minimised when c is chosen such that $\mathcal{R}$ is orthogonal to span$\{v_0, \ldots, v_{N-1}\}$.

The goal of DMD algorithm is to solve the eigenvalue problem of the companion matrix $\mathcal{S}$

$$V_1^N = \mathcal{A}V_0^{N-1} = V_0^{N-1}\mathcal{S} + \mathcal{R}, \quad (8)$$

where $\mathcal{S}$ approximates the eigenvalues of $\mathcal{A}$ when $\|\mathcal{R}\|_2 \to 0$.

The objective at this step is to solve the minimisation problem

$$\underset{\mathcal{S}}{\text{Minimise }} \mathcal{R} = \|V_1^N - V_0^{N-1}\mathcal{S}\|_2. \quad (9)$$

An estimate can be computed by multiplying V_1^N by the Moore–Penrose pseudoinverse of V_0^{N-1}:

$$\mathcal{S} = (V_0^{N-1})^+ V_1^N, \quad (10)$$

where $(V_0^{N-1})^+$ is computed according to Moore–Penrose pseudoinverse definition (Golub and Van Loan 1996).

The Moore–Penrose pseudoinverse approach might not be feasible when dealing with high dimensional non-intrusive data, as we previously pointed out in Bistrian and Navon (2015).

Following Schmid (2010), we developed an alternate algorithm based on singular value decomposition (SVD) of snapshot matrix V_0^{N-1}. This approach is helpful when the matrix V_0^{N-1} is rank deficient ($M > N$). The minimisation problem (9) has the following solution. We first identify a SVD of V_0^{N-1}:

$$V_0^{N-1} = U\Sigma W^H, \quad (11)$$

where U contains the proper orthogonal modes of V_0^{N-1}, Σ is a square diagonal matrix containing the singular values of V_0^{N-1} and W^H is the conjugate transpose of W.

Relations $\mathcal{A}V_0^{N-1} = V_1^N = V_0^{N-1}S + \mathcal{R}, \|\mathcal{R}\|_2 \to 0$ and $V_0^{N-1} = U\Sigma W^H$ yield

$$\mathcal{A}U\Sigma W^H = V_1^N = U\Sigma W^H S$$

$$\Rightarrow \quad U^H \mathcal{A}U\Sigma W^H = U^H U\Sigma W^H S$$

$$\Rightarrow \quad S = U^H \mathcal{A}U. \tag{12}$$

From $\mathcal{A}U\Sigma W^H = V_1^N$ it follows that $\mathcal{A}U = V_1^N W \Sigma^{-1}$ and hence

$$S = U^H(V_1^N W \Sigma^{-1}). \tag{13}$$

A direct consequence of solving the minimisation problem (9) is that decreasing the residual increases overall convergence and therefore the eigenvalues λ_j and the eigenvectors $\phi_j, j = 1, \ldots, N$ of $\mathcal{S}$ will converge toward the eigenvalues and the eigenvectors of the Koopman operator $\mathcal{A}$, respectively. More specifically, every column vector $v_i, i = 1, \ldots, N$ can be written as a linear combination of its predecessor:

$$v_i = \mathcal{A}v_{i-1} = \cdots = \mathcal{A}^{i-1}v_1, \quad i = 1, \ldots, N. \tag{14}$$

The eigenvectors of $\mathcal{S}$ form a basis for the span of $\mathcal{A}$, therefore, we can write every column vector as a linear combination of the eigenvectors

$$v_1 = \sum_{j=1}^{N} a_j \phi_j,$$

$$v_i = \sum_{j=1}^{N} \mathcal{A}^{i-1} a_j \phi_j, \quad i = 1, \ldots, N,$$

$$v_i = \sum_{j=1}^{N} a_j \lambda_j^{i-1} \phi_j, \quad i = 1, \ldots, N. \tag{15}$$

A straightforward interpretation of relations (15) brings the data snapshots at every time step $\{t_1, \ldots, t_N\}$ as a linear combination of DMD modes according to

$$v(t_i, \mathbf{x}) = \sum_{j=1}^{N} a_j \phi_j(\mathbf{x})\lambda_j^{i-1}, \quad i \in \{1, \ldots, N\},$$

$$t_i \in \{t_1, \ldots, t_N\}, \tag{16}$$

or in matrix formulation:

$$V_1^N = [v_1 \quad v_2 \quad \cdots \quad v_N]$$

$$= [\phi_1 \quad \phi_2 \quad \cdots \quad \phi_N] \begin{pmatrix} a_1 & & & \\ & a_2 & & \\ & & \ddots & \\ & & & a_N \end{pmatrix}$$

$$\times \begin{pmatrix} 1 & \lambda_1^1 & \lambda_1^2 & \cdots & \lambda_1^{N-1} \\ 1 & \lambda_2^1 & \lambda_2^2 & \cdots & \lambda_2^{N-1} \\ 1 & \vdots & \vdots & \vdots & \vdots \\ \vdots & \vdots & \vdots & \vdots & \vdots \\ 1 & \lambda_N^1 & \lambda_N^2 & \cdots & \lambda_N^{N-1} \end{pmatrix}, \tag{17}$$

where the right eigenvectors of $\mathcal{S}$, $\phi_j \in \mathbb{C}$ are *dynamic shape* (or Koopman) modes, the eigenvalues of $\mathcal{S}$, λ_j are called Ritz values (Chopra 2000) and coefficients $a_j \in \mathbb{C}$ are denoted as amplitudes or Koopman eigenfunctions. Each Ritz value $\lambda_j = e^{(\sigma_j + i\omega_j)\Delta t}$ is associated with the growth rate $\sigma_j = \log(|\lambda_j|)/\Delta t$ and the frequency $\omega_j = \arg(|\lambda_j|)/\Delta t$.

The modes' selection plays a central role in model reduction. The superposition of all Koopman modes, weighted by their amplitudes and complex frequencies, approximates the entire data sequence, but there are also modes that have a weak contribution. Our goal is to produce a ROM of the data involving only the most significant modes, having a strong contribution to the data representation, which we are calling *leading modes*.

Thus, the data snapshots at every time step $\{t_1, \ldots, t_N\}$ will be represented as a linear combination of the leading DMD modes according to

$$v_{\text{DMD}}(t_i, \mathbf{x}) = \sum_{j=1}^{k} a_j \phi_j(\mathbf{x})\lambda_j^{i-1}, \quad i \in \{1, \ldots, N\},$$

$$t_i \in \{t_1, \ldots, t_N\}, \tag{18}$$

where k represents the number of DMD modes involved in reconstruction of data snapshots, or in matrix formulation

$$V_1^N = [v_1 \quad v_2 \quad \cdots \quad v_N]$$

$$= [\phi_1 \quad \phi_2 \quad \cdots \quad \phi_k] \begin{pmatrix} a_1 & & & \\ & a_2 & & \\ & & \ddots & \\ & & & a_k \end{pmatrix}$$

$$\times \begin{pmatrix} 1 & \lambda_1^1 & \lambda_1^2 & \cdots & \lambda_1^{N-1} \\ 1 & \lambda_2^1 & \lambda_2^2 & \cdots & \lambda_2^{N-1} \\ 1 & \vdots & \vdots & \vdots & \vdots \\ \vdots & \vdots & \vdots & \vdots & \vdots \\ 1 & \lambda_k^1 & \lambda_k^2 & \cdots & \lambda_k^{N-1} \end{pmatrix}. \tag{19}$$

Here we point out that the k leading modes involved in ROM representation of data (19) are not the first k modes from representation (17). The leading modes represent a subset of DMD modes that will be selected from all computed DMD modes via several criteria, which will be the subject of discussion in the next section.

It can be seen that the SVD plays a central role in computing the DMD. In the present work, we propose a comparison between two DMD algorithms based on SVD. The first consists of a deterministic DMD method endowed with a vector filtering criterion to select the most influential modes. The second algorithm utilises an ARDMD to obtain the leading modes in the offline stage, that does not require an additional selection algorithm of the DMD modes. The two algorithms are presented in the following subsections.

2.2. Deterministic DMD with modes selection criterion (CrDMD)

We recently investigated different techniques of modes selection in DMD. Bistrian and Navon (2015) aimed to present a preliminary survey on DMD modes selection. We proposed a framework for modal decomposition of 2D flows, when numerical data are captured with large time steps. Key innovations for the DMD-based ROM introduced in Bistrian and Navon (2015) are the use of the Moore–Penrose pseudoinverse in the DMD computation that produced an accurate result and a novel selection method for the DMD modes. We eliminate the modes that contribute weakly to the data sequence based on the conservation of quadratic integral invariants (Navon and DeVilliers 1986) by the reduced order flow.

In Alekseev et al. (2016) we proposed a new framework for DMD based on the reduced Schmid operator. We investigated a variant of DMD algorithm and we explored the selection of the modes based on sorting them in decreasing order of their amplitudes. This procedure works well for models without modes that are very rapidly damped, having very high amplitudes. Therefore the selection of modes based on their amplitude is effective only in certain situations, as reported also by Noack, Morzynski, and Tadmor (2011).

In Bistrian and Navon (2017a) we focused on the effects of modes selection in DMD. We proposed a new vector filtering criterion for dynamic modes selection that is able to extract dynamically relevant flow features of time-resolved numerical data. The algorithm related in Bistrian and Navon (2017a) proposed a dynamic filtering criterion for which the amplitude of any mode is weighted by its growth rate. This method proved to be perfectly adapted to the flow dynamics, resulting in the identification of the most influential modes for the swirling flow investigated problems.

The first DMD algorithm we address in this survey is a deterministic (or classic) DMD based on the procedure introduced in Rowley et al. (2009). We apply this algorithm together with a vector filtering criterion for

selection of DMD modes involved in the ROM. This dynamic filtering criterion was proved to be perfectly adapted to the flow dynamics (Bistrian and Navon 2017a) and selects the modes which are dominant in both situations described above.

We define the amplification of any DMD mode as

$$A_j = \frac{1}{T} \int_0^T a_j \left(\lambda_j^{t/\Delta t} + \lambda_j^{-t/\Delta t} \right) dt$$
$$= \frac{a_j}{\sigma_j T} \left(e^{\sigma_j T} + e^{-\sigma_j T} - 2 \right), \quad j = 1, \ldots, N,$$
$$T = (N-1)\Delta t, \tag{20}$$

where λ_j are the Ritz values, $a_j \in \mathbb{C}$ are the modal amplitudes and $\sigma_j = \log(|\lambda_j|)/\Delta t$ represent the growth rates.

We define the relative error of the low-rank model as the L_2-norm of the difference between the flow variables and approximate DMD solutions over the exact one, that is,

$$Er_{\text{DMD}} = \frac{\| v(\mathbf{x}) - v_{\text{DMD}}(\mathbf{x}) \|_2}{\| v(\mathbf{x}) \|_2}, \tag{21}$$

where $v(\mathbf{x})$ represent the numerical data and $v_{\text{DMD}}(\mathbf{x})$ represent the low-rank DMD approximation.

We retain dynamic modes and associated frequencies in descending order of their amplification defined by (20) until a minimum relative error of reconstruction is achieved. To produce the ROM amounts to finding the solution to the following minimisation problem:

$$\text{Find}_{k \in \mathbb{N}, k \geq 2} \quad v_{\text{DMD}}(t_i, \mathbf{x}) = \sum_{j=1}^k a_j \phi_j(\mathbf{x}) \lambda_j^{i-1},$$
$$i \in \{1, \ldots, N\}, \ t_i \in \{t_1, \ldots, t_N\},$$
$$\text{Subject to} \quad \arg\min_k \{A_1 > A_2 > \cdots > A_k,$$
$$Er_{\text{DMD}} \leq \varepsilon \}, \quad \varepsilon = 10^{-5}. \tag{22}$$

Consequently, the modes and frequencies that have the strongest influence on the quality of approximation are selected to be included in the ROM. The CrDMD algorithm is presented below.

Consequently, the modes and frequencies that have the strongest influence on the quality of approximation are selected to be included in the ROM.

2.3. Adaptive randomised DMD

The SVD plays a central role in computing the DMD. Therefore, the Moore–Penrose pseudoinverse approach we previously employed in Bistrian and Navon (2015) might not be feasible when dealing with high dimensional non-intrusive data. It is more desirable to reduce

Algorithm 1 (CrDMD): Deterministic DMD algorithm with modes selection criterion

Initial data: $V_0^{N-1} \in \mathbb{R}^{M \times N}$, $V_1^N \in \mathbb{R}^{M \times N}$.

1. Produce the economy-size SVD: $[U, \Sigma, W] = SVD(V_0^{N-1})$, where U contains the proper orthogonal modes of V_0^{N-1} and Σ contains the singular values.
2. Solve the minimisation problem (9): $S = U^H(V_1^N W \Sigma^{-1})$.
3. Compute dynamic modes solving the eigenvalue problem $SX = X\Lambda$ and obtain dynamic modes as $\Phi = UX$. The diagonal entries of Λ represent the eigenvalues λ.
4. Project dynamic modes onto the first snapshot to calculate the vector containing dynamic modes amplitudes $Ampl = (a_j)_{j=1}^{rank(\Lambda)}$.
5. Solve the minimisation problem (22) and obtain the rank k. Retain dynamic modes and associated frequencies in descending order of their amplification defined by (20).
6. The reconstructed data at every time step $\{t_1, \ldots, t_N\}$ involving the selected DMD modes is given by the product

$$V^{\text{DMD}} = \Phi \cdot diag\left(Ampl\right) \cdot Van =$$

$$= \begin{bmatrix} \phi_1 & \phi_2 & \cdots & \phi_k \end{bmatrix} \begin{pmatrix} a_1 & & & \\ & a_2 & & \\ & & \ddots & \\ & & & a_k \end{pmatrix}$$

$$\times \begin{pmatrix} 1 & \lambda_1^1 & \lambda_1^2 & \ldots & \lambda_1^{N-1} \\ 1 & \lambda_2^1 & \lambda_2^2 & \ldots & \lambda_2^{N-1} \\ 1 & \vdots & \vdots & \vdots & \vdots \\ \vdots & \vdots & \vdots & \vdots & \vdots \\ 1 & \lambda_k^1 & \lambda_k^2 & \ldots & \lambda_k^{N-1} \end{pmatrix} \quad (23)$$

Output: k, V_{DMD}.

---

the problem dimension to avoid a computationally expensive SVD. We have introduced in Bistrian and Navon (2017b) the procedure of randomisation of data prior to SVD. Thus, we endow the DMD algorithm with a randomised SVD function adapted after Halko, Martinsson, and Tropp (2011), aiming to improve the accuracy of the reduced order linear model and to reduce the CPU time.

We developed a randomised DMD as a fast and accurate option in model order reduction of non-intrusive data. To the best of our knowledge, Bistrian and Navon (2017b) was the first to introduce the randomised DMD algorithm with application to fluid dynamics, after the randomised SVD algorithm recently introduced in Erichson and Donovan (2016) for processing of high-resolution videos.

The rank of the reduced DMD model is given such that the relative error of data reconstruction becomes sufficiently small. We recall this procedure as *ARDMD*. Determination of the optimal rank k of the reduced DMD model then amounts to finding the solution to the following optimisation problem:

$$\underset{k \in \mathbb{N}, k \geq 2}{\text{Find}} \quad v_{\text{DMD}}(t_i, \mathbf{x}) = \sum_{j=1}^{k} a_j \phi_j(\mathbf{x}) \lambda_j^{i-1},$$

$$i \in \{1, \ldots, N\}, t_i \in \{t_1, \ldots, t_N\},$$

$$\text{Subject to} \quad k = \arg\min\{Er_{\text{DMD}} \leq \varepsilon\}, \quad (24)$$

where Er_{DMD} is the relative error of the low-rank model defined by Equation (21), $\varepsilon = 10^{-5}$ represents a constant that sets the admissible limit for the relative error of data reconstruction. The accuracy of the numerical procedure can be adjusted according to the value chosen for this parameter.

The ARDMD algorithm (Algorithm 2) is presented below.

The first major advantage of the ARDMD proposed in this paper is represented by the fact that ARDMD produces a reduced order subspace of Ritz values, having the same dimension as the rank of RSVD function. As a consequence, after solving the optimisation problem (24), an additional selection criterion of the Ritz values associated with their DMD modes is no longer needed. We employ in the flow reconstruction the most significant DMD modes associated with their amplitudes and Ritz values, respectively, leading to the minimum error of flow reconstruction, due to the adaptive feature of the proposed algorithm.

The second major improvement offered by the proposed randomised DMD can be found in the significant reduction of CPU time for computation of massive numerical data, as we will detail in the section dedicated to numerical results.

3. Numerical results

In the following we present numerical results demonstrating the computational performance of the two algorithms: CrDMD and ARDMD, respectively. The test problem used in this paper consists of the non-linear Saint-Venant equations (also called the shallow water equations Saint-Venant and Barré 1871) in a channel on

---

Algorithm 2 (ARDMD): Adaptive randomised DMD algorithm

Initial data: $V_0^{N-1} \in \mathbb{R}^{M \times N}$, $V_1^N \in \mathbb{R}^{M \times N}$, $M \geq N$, integer target rank $k \geq 2$ and $k < N$.

1. For $k = 2$ to $N - 1$.
2. Produce the randomised SVD:

$$[U, \Sigma, W] = \mathbf{RSVD}\left(V_0^{N-1}, k\right),$$

   where U contains the proper orthogonal modes of V_0^{N-1} and Σ contains the singular values. The RSVD function is described in continuation of this algorithm.
3. Solve the minimisation problem (9): $S = U^H(V_1^N W \Sigma^{-1})$.
4. Solving the eigenvalue problem $[X, \Lambda] = eig(S)$, obtain dynamic modes as $\Phi = UX$. The diagonal entries of Λ represent the eigenvalues λ.
5. Project dynamic modes onto the first snapshot to calculate the vector containing dynamic modes amplitudes $Ampl = (a_j)_{j=1}^{rank(\Lambda)}$.
6. The DMD model of rank k is given by the product

$$V^{\mathrm{DMD}} = \Phi \cdot diag\left(Ampl\right) \cdot Van == \begin{bmatrix} \phi_1 & \phi_2 & \cdots & \phi_k \end{bmatrix} \begin{pmatrix} a_1 & & & \\ & a_2 & & \\ & & \ddots & \\ & & & a_k \end{pmatrix} \times \begin{pmatrix} 1 & \lambda_1^1 & \lambda_1^2 & \cdots & \lambda_1^{N-1} \\ 1 & \lambda_2^1 & \lambda_2^2 & \cdots & \lambda_2^{N-1} \\ 1 & \vdots & \vdots & \vdots & \vdots \\ \vdots & \vdots & \vdots & \vdots & \vdots \\ 1 & \lambda_k^1 & \lambda_k^2 & \cdots & \lambda_k^{N-1} \end{pmatrix} \tag{25}$$

7. Solve the optimisation problem (24) and obtain the lowest rank k and the k leading DMD modes.
8. Finalise the ROM at every time step $\{t_1, \ldots, t_N\}$, involving the leading k DMD modes, with the product given by Equation (25).
   Output: k, V_{DMD}.

Randomised SVD function (RSVD):

Initial data: $V_0^{N-1} \in \mathbb{R}^{M \times N}$, $M \geq N$, integer target rank $k \geq 2$ and $k < N$.

1. Generate random test matrix $M = rand(N, r)$, $r = \min(N, 2k)$.
2. Compute the sampling matrix by multiplication of snapshot matrix with random matrix $Q = V_0^{N-1}M$.
3. Orthonormalisation of sampling matrix via Gram–Schmidt orthonormal method $Q \leftarrow GramSchmidt(Q)$.
4. Projection of snapshot matrix to smaller space $V = Q^H V_0^{N-1}$, where H denotes the conjugate transpose.
5. Produce the economy-size SVD of low-dimensional snapshot matrix $[Q_1, \Sigma, W] = SVD(V)$.
6. Compute the right singular vectors $U = QQ_1$.
   Output: Procedure returns $U \in \mathbb{R}^{M \times k}$, $\Sigma \in \mathbb{R}^{k \times k}$, $W \in \mathbb{R}^{N \times k}$.

---

the rotating earth:

$$\frac{\partial\left(\tilde{u}\tilde{h}\right)}{\partial t} + \frac{\partial\left(\tilde{u}^2\tilde{h} + g\tilde{h}^2/2\right)}{\partial x} + \frac{\partial\left(\tilde{u}\tilde{v}\tilde{h}\right)}{\partial y}$$

$$= \tilde{h}\left(f\tilde{v} - g\frac{\partial H}{\partial x}\right), \tag{26}$$

$$\frac{\partial\left(\tilde{v}\tilde{h}\right)}{\partial t} + \frac{\partial\left(\tilde{u}\tilde{v}\tilde{h}\right)}{\partial x} + \frac{\partial\left(\tilde{v}^2\tilde{h} + g\tilde{h}^2/2\right)}{\partial y}$$

$$= \tilde{h}\left(-f\tilde{u} - g\frac{\partial H}{\partial y}\right), \tag{27}$$

$$\frac{\partial\tilde{h}}{\partial t} + \frac{\partial\left(\tilde{u}\tilde{h}\right)}{\partial x} + \frac{\partial\left(\tilde{v}\tilde{h}\right)}{\partial y} = 0, \tag{28}$$

where $\tilde{u}$ and $\tilde{v}$ are the velocity components in the $\tilde{x}$ and $\tilde{y}$ axis directions respectively, $\tilde{h}$ represents the depth of the fluid, $H(x, y)$ is the orography field, $\tilde{f}$ is the Coriolis factor and g is the acceleration of gravity.

The Saint-Venant equations, named after the French mathematician Adhémar Jean Claude Barré de Saint-Venant (1797–1886), represent a system of conservation laws that describe the flow below a pressure surface in a fluid. A description of the Saint-Venant system as a result of depth-integration of the Navier–Stokes equations is posed by Saint-Venant and Barré (1871). Details can be found in Navon (1979), Vreugdenhil (1994) and Galdi (1994).

We consider that the reference computational configuration is the rectangular 2D domain $\Omega = [0, L_{\max}] \times [0, D_{\max}]$. Subscripts represent the derivatives with respect to time and the streamwise and spanwise coordinates.

In this model, the Coriolis parameter is modelled as varying linearly in the spanwise direction, such that

$$\tilde{f} = f_0 + \beta(\tilde{y} - D_{\max}), \tag{29}$$

where f_0, β are constants, $L_{\max}, D_{\max}$ are the dimensions of the rectangular domain of integration. The height of the orography is given by the fixed two-dimensional field

$$H(x, y) = \alpha e^{y^2 - x^2}. \tag{30}$$

The model (26)–(28) is associated with periodic boundary conditions in the $\tilde{x}$-direction and solid wall boundary condition in the $\tilde{y}$-direction:

$$\tilde{u}(0, \tilde{y}, \tilde{t}) = \tilde{u}(L_{\max}, \tilde{y}, \tilde{t}), \ \tilde{v}(\tilde{x}, 0, \tilde{t})$$
$$= \tilde{v}(\tilde{x}, D_{\max}, \tilde{t}) = 0, \tag{31}$$

and also with the initial condition of Grammeltvedt (1969) as the initial height field, which propagates the energy in wave number one, in the streamwise direction:

$$h_0(\tilde{x}, \tilde{y}) = H_0 + H_1 \tanh\left(\frac{9(D_{\max}/2 - \tilde{y})}{2D_{\max}}\right) + H_2 \sin$$
$$\times \left(\frac{2\pi\tilde{x}}{L_{\max}}\right) \cosh^{-2}\left(\frac{9(D_{\max}/2 - \tilde{y})}{D_{\max}}\right). \tag{32}$$

Using the geostrophic relationship $\tilde{u} = -\tilde{h}_{\tilde{y}}(g/\tilde{f})$, $\tilde{v} = \tilde{h}_{\tilde{x}}(g/\tilde{f})$, the initial velocity fields are derived as

$$u_0(\tilde{x}, \tilde{y}) = -\frac{g}{\tilde{f}}\frac{9H_1}{2D_{\max}}\left(\tanh^2\left(\frac{9D_{\max}/2 - 9\tilde{y}}{2D_{\max}}\right) - 1\right)$$
$$- \frac{18g}{\tilde{f}}H_2 \sinh\left(\frac{9D_{\max}/2 - 9\tilde{y}}{D_{\max}}\right)$$

$$\times \frac{\sin\left(\frac{2\pi\tilde{x}}{L_{\max}}\right)}{D_{\max}\cosh^3\left(\frac{9D_{\max}/2 - 9\tilde{y}}{D_{\max}}\right)}, \tag{33}$$

$$v_0(\tilde{x}, \tilde{y}) = 2\pi H_2 \frac{g}{\tilde{f}L_{\max}} \cos\left(\frac{2\pi\tilde{x}}{L_{\max}}\right) \cosh^{-2}$$
$$\times \left(\frac{9(D_{\max}/2 - \tilde{y})}{D_{\max}}\right). \tag{34}$$

The constants used for the test model are

$$f_0 = 10^{-4}\,\text{s}^{-1}, \alpha = 4000,$$
$$\beta = 1.5 \times 10^{-11}\,\text{s}^{-1}\,\text{m}^{-1}, \quad g = 9.81 s^{-1}\,\text{m}\,\text{s}^{-1},$$
$$D_{\max} = 50 \times 10^3\,\text{m}, \quad L_{\max} = 254 \times 10^3\text{m},$$
$$H_0 = 10 \times 10^3\,\text{m}, \quad H_1 = -400\,\text{m}, \quad H_2 = -300\,\text{m}.$$

We set the error of the numerical algorithms to be less than $\varepsilon = 10^{-5}$. To measure the accuracy of the reduced shallow water model, we undertake a non-dimensional analysis of the shallow water model. Following Barenblatt (1996), reference quantities of the dependent and independent variables in the shallow water model are considered, i.e. the length scale $L_{ref} = L_{\max}$ and the reference units for the height and velocities, respectively, are given by the initial conditions $h_{\text{ref}} = h_0$, $u_{\text{ref}} = u_0$. A typical time scale is also considered, assuming the form $t_{\text{ref}} = L_{\text{ref}}/u_{\text{ref}}$. In order to make the system of Equations (26)–(28) non-dimensional, we define the non-dimensional variables

$$(t, x, y) = \left(\tilde{t}/t_{\text{ref}}, \tilde{x}/L_{\text{ref}}, \tilde{y}/L_{\text{ref}}\right),$$
$$(h, u, v) = \left(\tilde{h}/h_{\text{ref}}, \tilde{u}/u_{\text{ref}}, \tilde{v}/u_{\text{ref}}\right).$$

The numerical results are obtained employing a Lax–Wendroff finite difference discretisation scheme and used in further numerical experiments in dimensionless form.

We will evaluate the behaviour of the two algorithms by conducting two numerical experiments. In the first numerical experiment, the training data comprises a number of 145 unsteady solutions of the two-dimensional shallow water equations model (26)–(28), at regularly spaced time intervals of $\Delta t = 3600$ s for each solution variable.

To perform the comparison between the DMD algorithms presented herein, we illustrate in Figures 1–3 the spectra of DMDs of geopotential height field h, streamwise field u and spanwise field v, respectively, in case of DMD with modes selection criterion (Algorithm 1-CrDMD) and adaptive randomised DMD (Algorithm 2-ARDMD). The figures highlight the effect of the presented algorithms to select different modes, having the
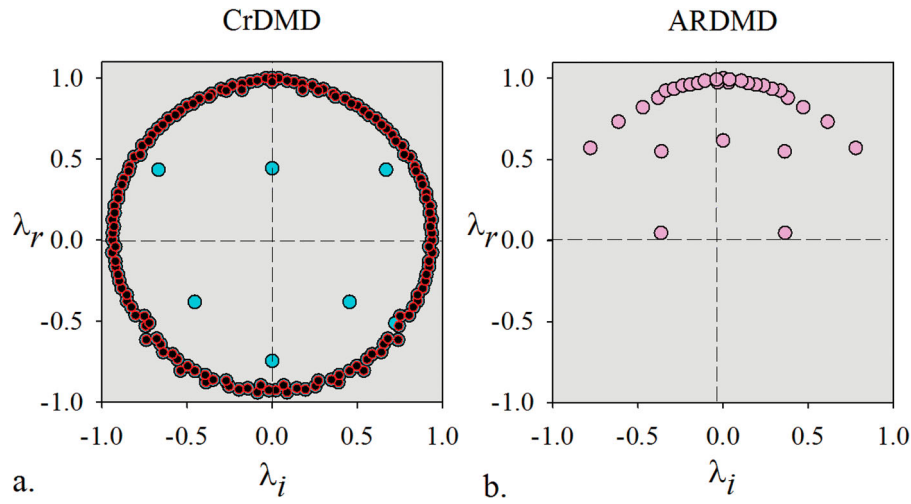
Figure 1. The spectrum of DMD of height field h in case of: (a) DMD with modes selection criterion – CrDMD: 144 modes (lighter dots), 137 modes selected for ROM (darker dots), (b) adaptive randomised DMD – ARDMD: 30 modes selected for ROM.
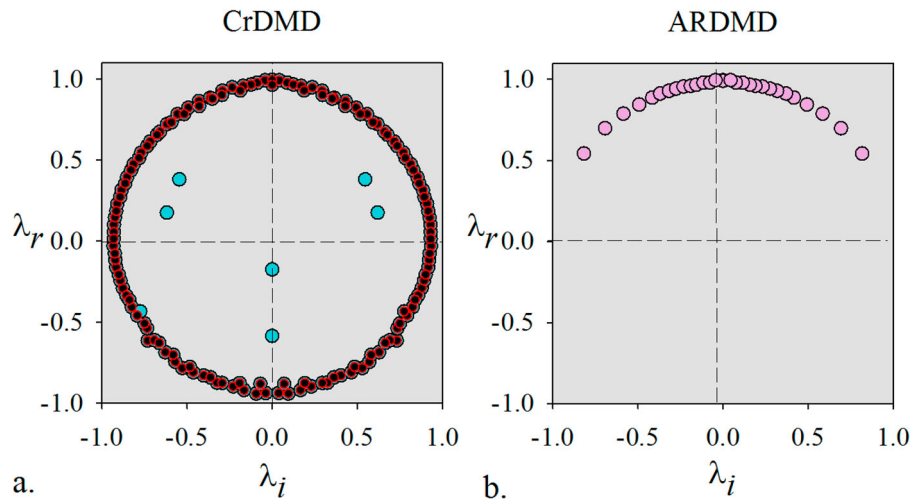
Figure 2. The spectrum of DMD of streamwise field u in case of: (a) DMD with modes selection criterion – CrDMD: 144 modes (lighter dots), 137 modes selected for ROM (darker dots), (b) adaptive randomised DMD – ARDMD: 30 modes selected for ROM.
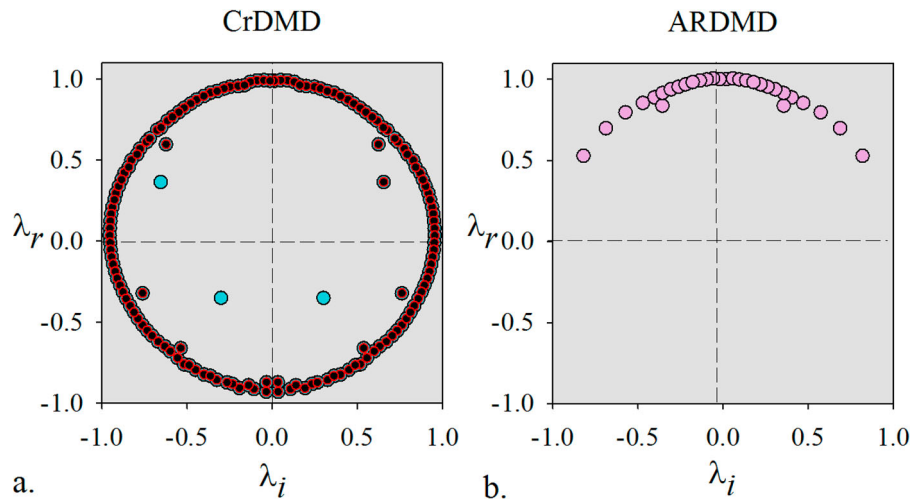
Figure 3. The spectrum of DMD of spanwise field v in case of: (a) DMD with modes selection criterion – CrDMD: 144 modes (lighter dots), 137 modes selected for ROM (darker dots), (b) adaptive randomised DMD – ARDMD: 30 modes selected for ROM.

Table 1. Comparison of the efficiency of the two algorithms, $\Delta t = 3600$ s, 145 data snapshots have been processed.

Algorithm	Computed DMD modes	The ROM rank	The relative error
CrDMD[a]	144	$k = 137$	$Er^h_{DMD} = 2.8362 \times 10^{-6}$
ARDMD[b]	30	$k = 30$	$Er^h_{DMD} = 2.7189 \times 10^{-6}$

[a] DMD with modes selection criterion.
[b] Adaptive randomised dynamic mode decomposition.

strongest impact on the reconstruction of the flow dynamics.

Table 1 presents the number of DMD modes computed and involved in the ROM, provided by the two algorithms, respectively and the relative error Er_{DMD} of reconstruction of the flow field.

Obviously, when the classic DMD algorithm is applied, the practitioner has to address a modes' selection method. In the case of a deterministic algorithm **CrDMD**, we solved the constrained optimisation problems described by Equation (22) employing the sequential quadratic programming (SQP) (Nocedal and Wright 2006). The number of selected modes for representation of h, u, v fields by the reduced DMD model are presented in Table 1 and illustrated in Figures 1(a)–3(a), where lighter circles represent total computed modes (144 modes), while darker circles represent the retained

modes after DMD optimisation (137 modes). In case of application of dynamic vector filtering criterion (22), the dominant modes are included in a smaller subspace, preserving a very good approximation of the full solution by the ROM model. The benefit of the proposed filtering criterion consists in eliminating the DMD modes that contribute weakly to the data sequence. It provides an automatic selection of the most representative modes, even when they exhibit rapid growth with lower amplitudes or they consist of high amplitudes fast damped modes.
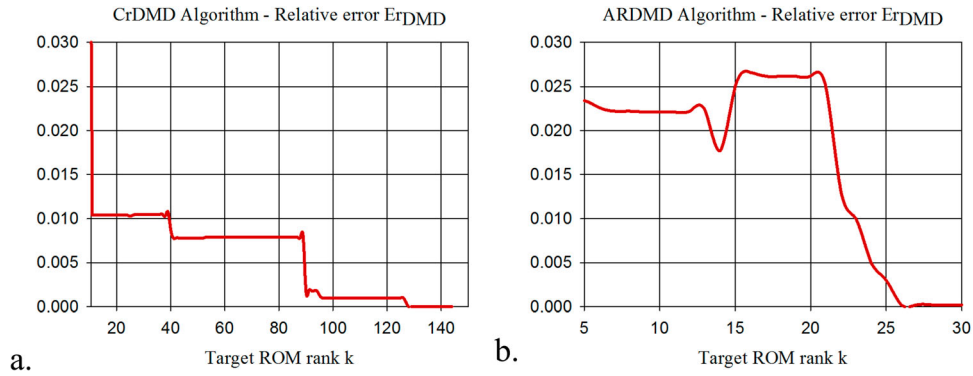
Compared to the **CrDMD** algorithm, the randomised DMD algorithm **ARDMD** produces a significantly reduced size spectrum which elegantly incorporates the most influential modes. The first major advantage of the adaptive randomised algorithm **ARDMD** consists in producing a reduced order subspace of Ritz values, which has the same dimension as the rank of randomised SVD function, where the most significant modes live. As a consequence, this procedure omits a further selection criterion of the Ritz values. The optimal rank of the ROM model is the unique solution to the optimisation problem (24). We have tested several global optimisation methods such as genetic algorithm combined with sequential quadratic programming (GA-SQP) (Nocedal and Wright 2006) and simulated annealing
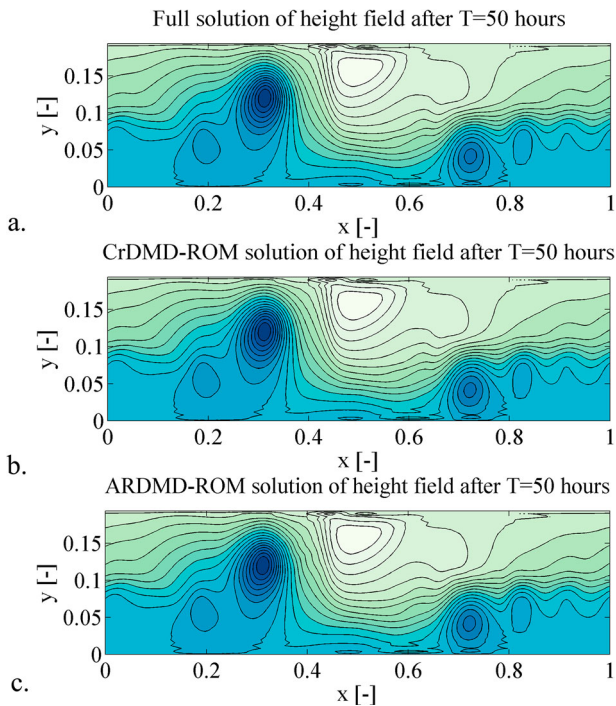
Figure 4. (a) Full solution of height field after $T = 50$ h; (b) ROM solution of height field obtained with CrDMD algorithm ($k = 137$ modes); (c) ROM solution of height field obtained with ARDMD algorithm ($k = 30$ modes). The relative error is of order $\mathcal{O}(10^{-6})$ in both cases.
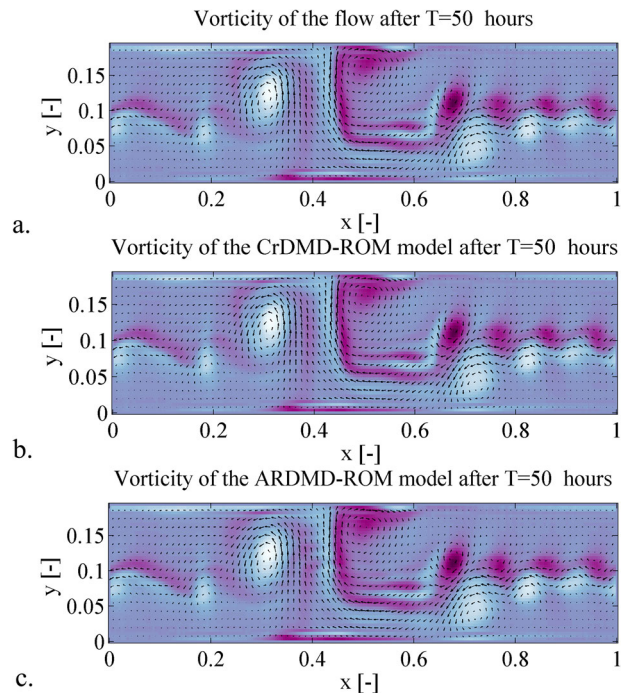
Figure 5. (a) Vorticity field after $T = 50$ h; (b) ROM solution of vorticity field obtained with CrDMD algorithm ($k = 137$ modes); (c) ROM solution of vorticity field obtained with ARDMD algorithm ($k = 30$ modes). The relative error is of order $\mathcal{O}(10^{-6})$ in both cases.

Figure 6. The relative errors computed with respect to the ROM rank, in case of application of: (a) deterministic DMD with modes selection criterion **CrDMD** and (b) adaptive randomised DMD algorithm **ARDMD**, $\Delta t = 3600$ s, 145 data snapshots have been processed.

(SA) (Navon, Brown, and Robertson 1990; Yang 2010), to solve the optimisation problem (24), with similar computational difficulties. In this work, a collaborative optimisation technique involving hybrid simulated annealing and sequential quadratic programming (SA-SQP-CO) (Cao et al. 2015) is chosen because it ensures the existence of the solution to the optimisation problem (24). The SA-SQP-CO method and its convergence efficiency are fully detailed in Cao et al. (2015).

Another benefit of the randomised DMD is that the low order solution (18) is guaranteed to satisfy the boundary conditions (31) of the full model, because the DMD modes provided by the **ARDMD** algorithm satisfy the relations

$$\phi_j^u(0,y) = \phi_j^u(L_{\max}, y), \quad j = 1, \ldots, k, \qquad (35)$$

$$\phi_j^v(x,0) = \phi_j^v(x, D_{\max}) = 0, \quad j = 1, \ldots, k, \qquad (36)$$

where ϕ_j^u, ϕ_j^v are dynamic modes of the u and v fields, respectively, and k represents the number of the retained modes in the ROM.

The representation of the height field, based on the selected modes in case of algorithms **CrDMD** and **ARDMD** is displayed, respectively, in Figure 4. The vorticity field is illustrated in Figure 5, computed with the two algorithms. The ROM exhibits a relative error of order $\mathcal{O}(10^{-6})$ in both cases.

As seen so far, both algorithms produce ROMs with a preset desired error, but they have different ranks. The relative error of the ROM model with respect to the rank is illustrated in Figure 6 in the case of application of the two algorithms.

Data presented in Figure 6 confirms the efficiency of the **ARDMD** algorithm. Although the previous techniques detailed in Bistrian and Navon (2015), Alekseev et al. (2016), and Bistrian and Navon (2017a) lead to a reduced number of retained modes, there are still

missing modes that would contribute to data approximation. Hence the relative error of flow reconstruction by the ROM is the best in the case of randomised DMD. The great advantage of adaptive randomised DMD algorithm **ARDMD** is that it avoids the computational efforts required for implementing an additional criterion of influential modes'selection, since they are automatically selected.

Thus a significant reduction in computational time is also achieved compared with deterministic DMD associated with different modes of selection criteria. The CPU time required in the offline stage is presented in Figure 7. By employing the randomised DMD algorithm **ARDMD** in comparison with deterministic DMD associated with the energetic criterion for modes selection **CrDMD**, the computational complexity of the low order model is significantly reduced from the very beginning, as illustrated in Figure 7. Figures 8 and 9 present some examples of DMD modes involved in the ROM, in case of application of the two aforementioned algorithms.
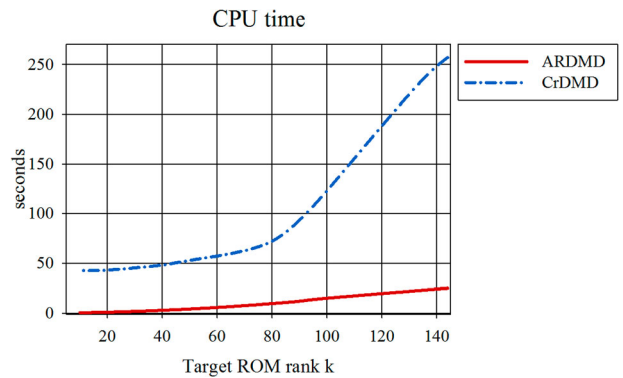
Figure 7. The CPU time required in the offline stage by applying adaptive randomised DMD **ARDMD** and deterministic DMD associated with the energetic criterion for modes selection **CrDMD**, $\Delta t = 3600$ s, 145 data snapshots have been processed.
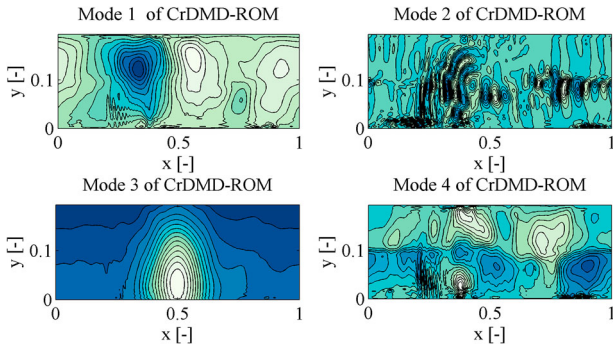
Figure 8. Examples of DMD modes computed with **CrDMD** algorithm, which are involved in the ROM model.
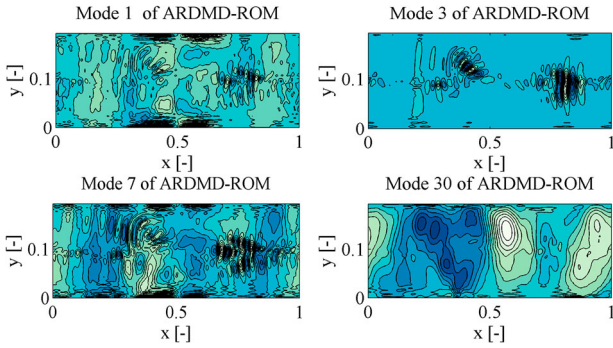
Figure 9. Examples of DMD modes computed with **ARDMD** algorithm, which are involved in the ROM model.

In the second numerical experiment, we consider that a larger amount of data is processed with the two algorithms. The training data comprises now a number of 289 unsteady solutions of the two-dimensional shallow water equations model (26)–(28), at regularly spaced time intervals of $\Delta t = 1800$ s for each solution variable.

The relative error of the ROM model with respect to its rank is illustrated in Figure 10 in the case of application of the two algorithms.
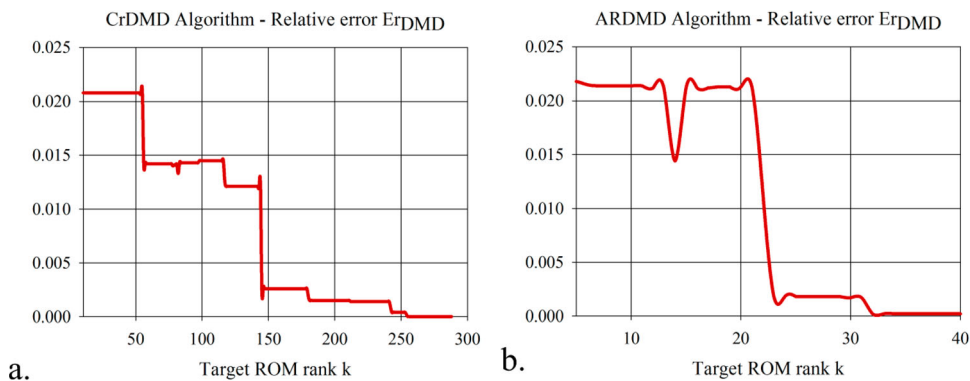
Table 2. Comparison of the efficiency of the two algorithms, $\Delta t = 1800$ s, 289 data snapshots have been processed.

Algorithm	Computed DMD modes	The ROM rank	The relative error
CrDMD[a]	288	$k = 255$	$Er^h{}_{DMD} = 3.7314 \times 10^{-6}$
ARDMD[b]	32	$k = 32$	$Er^h{}_{DMD} = 2.9743 \times 10^{-6}$

[a] DMD with modes selection criterion.
[b] Adaptive randomised dynamic mode decomposition.

Table 2 presents the number of DMD modes computed and involved in the ROM, provided by the two algorithms, respectively and the relative error Er_{DMD} of reconstruction of the flow field, when 289 snapshots data are processed.

The number of selected modes for representation of h,u,v fields by the reduced DMD model in the case of deterministic algorithm **CrDMD** is $k = 255$, while the randomised algorithm **ARDMD** selects a number of $k = 32$ leading modes for ROM. Through an efficient selection of the important modes, we have achieved a nine times smaller model compared to the total number of data snapshots.

The vorticity field after $T = 35$ h is illustrated in Figure 11, computed with the two algorithms, employing $k = 255$ modes with CrDMD algorithm, and $k = 32$ modes with ARDMD algorithm. The ROM exhibits a relative error of order $\mathcal{O}(10^{-6})$ in both cases.

The efficiency of the adaptive randomised DMD algorithm is illustrated also by the CPU time, depicted in Figure 12. In case of processing a large amount of data (289 data snapshots have been processed in the second numerical experiment), the **ARDMD** which requires no selection criteria is highly more efficient than the deterministic **CrDMD** with the energetic criterion for modes selection.

After the DMD modes involved in the ROM have been calculated, the coefficients of the ROM of state solutions can be estimated for the entire time window

Figure 10. The relative errors computed with respect to the ROM rank, in case of application of: (a) deterministic DMD with modes selection criterion **CrDMD** and (b) adaptive randomised DMD algorithm **ARDMD**, $\Delta t = 1800$ s, 289 data snapshots have been processed.
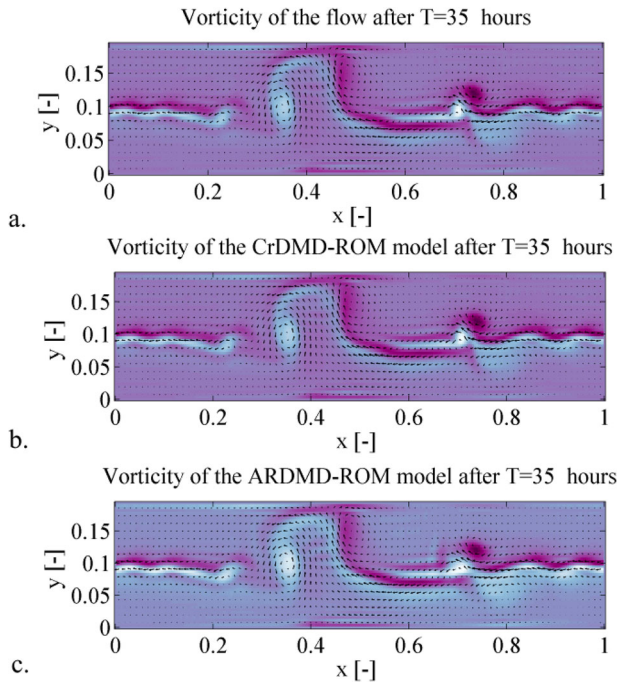
Figure 11. (a) Vorticity field after $T = 35$ h, $\Delta t = 1800$ s; (b) ROM solution of vorticity field obtained with CrDMD algorithm ($k = 255$ modes); (c) ROM solution of vorticity field obtained with ARDMD algorithm ($k = 32$ modes). The relative error is of order $\mathcal{O}(10^{-6})$ in both cases.
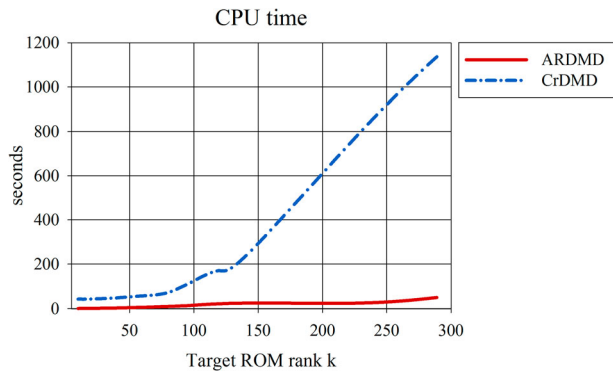
Figure 12. The CPU time required in the offline stage by applying adaptive randomised DMD **ARDMD** and deterministic DMD associated with the energetic criterion for modes selection **CrDMD**, $\Delta t = 1800$ s.

by interpolating the DMD computed coefficients using radial basis functions (RBF) discussed in Bistrian and Navon (2015, 2017a) or kriging techniques (Krige 1951; Wahba 1990).

4. Summary and conclusions

The present investigation has focused on a subject of great interest in fluid dynamics: identification of a ROM from numerical code output by non-intrusive techniques (i.e. not requiring projecting of the governing equations

onto the reduced basis modes, assuming that these governing equations or their numerical code are not available).

We performed a comparison between two methods of model order reduction based on DMD. The first method is a deterministic (classic) DMD technique endowed with a dynamic filtering criterion of selection of modes used in the ROM model (**CrDMD**). The second method is an adaptive randomised DMD algorithm (**ARDMD**) based on a randomised SVD.

In order to compare the performances of the proposed algorithms, we performed the model order reduction of non-intrusive data originating from the Saint-Venant model (or shallow water equations).

Unlike the classic selection based on modes amplitude, dynamic vector filtering criterion **CrDMD** offers two major advantages: it provides an automatic selection of the most representative modes, even when they exhibit rapid growth with lower amplitudes or they are high amplitudes fast damped modes. The **CrDMD** algorithm proved its efficiency in application to shallow water equations model, preserving a very good approximation of the full solution by the ROM model.

To overcome the inconveniences of developing and implementing a mode selection criterion associated with DMD, we developed a novel technique based on randomised DMD as a fast and accurate option in model order reduction. The adaptive randomised DMD algorithm (**ARDMD**) is endowed with an RSVD function. The rank of the ROM is given as the unique solution of an optimisation problem whose constraints consist of a sufficiently small relative error of data reconstruction and a sufficiently high correlation coefficient between the numerical data and the DMD solution. Solving the optimisation problem (24) using a collaborative optimisation technique involving hybrid simulated annealing and sequential quadratic programming (SA-SQP-CO) (Cao et al. 2015) we gain a fast and accurate adaptive randomised DMD algorithm, with a significantly lower rank for the new ROM, compared to the case of the deterministic **CrDMD** algorithm with modes selection criterion.

The major advantages of the adaptive randomised DMD (**ARDMD**) are:

- This method provides an efficient tool in developing the linear model of a complex flow field described by non-linear models or non-intrusive data.
- This method does not require an additional selection algorithm of the DMD modes. ARDMD produces a reduced order subspace of Ritz values, having the same dimension as the rank of randomised

SVD function, where the most significant DMD modes live.

- The low order solution (18) is guaranteed to satisfy the boundary conditions (31) of the full model.
- We gain a significant reduction of the offline CPU time in the computation of the ROM compared with the classic DMD associated with different modes of selection criteria.

In the first numerical experiment, we consider 145 data snapshots at regularly spaced time intervals of $\Delta t = 3600$ s for each solution variable. The numerical results presented in Table 1 show that both aforementioned algorithms provide an accurate ROM, the relative error being of order $\mathcal{O}(10^{-6})$ in both cases. But the rank of the ROM produced by the adaptive randomised **ARDMD** algorithm is four and a half times smaller than in the case of the deterministic algorithm with a selection criterion **CrDMD**. Hence the conclusion that the adaptive randomised DMD method is much more effective in the selection of significant DMD modes which are involved in the ROM and it has computational advantages over previously suggested deterministic DMD.

The efficiency of the adaptive randomised DMD method is especially evident in the case of large amount of snapshots data. In the second numerical experiment, we double the amount of data and we consider 289 data snapshots at regularly spaced time intervals of $\Delta t = 1800$ s. The rank of the ROM produced by the adaptive randomised **ARDMD** algorithm is eight times smaller than in the case of the deterministic algorithm with a selection criterion **CrDMD** and nine times smaller compared to the total number of data snapshots.

Randomised algorithms quickly prove their utility in reduced-order modelling. Recently, Pendergrass et al. (2016) introduced a GPU accelerated implementation of SVD and DMD and Erichson et al. (2017) proposed a randomised algorithm for computing the low-rank DMD for large-scale data.

Application of the adaptive randomised DMD algorithm to shallow water equations model offers the main advantage of deriving a ROM capable to provide a variety of information describing the behaviour of the flow field. However, the results are model dependent. A future extension of this research will address randomised algorithms for modal decomposition of swirling flows, where a large amount of data will be processed. A rigorous algorithm efficiency analysis will be also performed based on the convergence rates of the Kolmogorov n-widths (Cacuci, Navon, and Ionescu–Bujor 2014).

ORCID

D. A. Bistrian 🆔 http://orcid.org/0000-0001-8957-5879
I. M. Navon 🆔 http://orcid.org/0000-0001-7830-7094

References

Alekseev, A. K., D. A. Bistrian, A. E. Bondarev, and I. M. Navon. 2016. "On Linear and Nonlinear Aspects of Dynamic Mode Decomposition." *International Journal for Numerical Methods in Fluids* 82: 348–371.

Bagheri, S. 2013. "Koopman-mode Decomposition of the Cylinder Wake." *Journal of Fluid Mechanics* 726: 596–623.

Balajewicz, M. J., E. H. Dowell, and B. R. Noack. 2013. "Low-dimensional Modelling of High-Reynolds-number Shear Flows Incorporating Constraints from the Navier–Stokes Equation." *Journal of Fluid Mechanics* 729: 285–308.

Barenblatt, G. I. 1996. *Scaling, Self-similarity, and Intermediate Asymptotics*. Cambridge Texts in Applied Mathematics. Cambridge: Cambridge University Press.

Berger, E., M. Sastuba, D. Vogt, B. Jung, and H. Ben Amor. 2014. "Dynamic Mode Decomposition for Perturbation Estimation in Human Robot Interaction." The 23rd IEEE International Symposium on Robot and Human Interactive Communication, Edinburgh, August, 593–600.

Bistrian, D. A., and I. M. Navon. 2015. "An Improved Algorithm for the Shallow Water Equations Model Reduction: Dynamic Mode Decomposition vs POD." *International Journal for Numerical Methods in Fluids* 78 (9): 552–580.

Bistrian, D. A., and I. M. Navon. 2017a. "The Method of Dynamic Mode Decomposition in Shallow Water and a Swirling Flow Problem." *International Journal for Numerical Methods in Fluids* 83: 73–89.

Bistrian, D. A., and I. M. Navon. 2017b. "Randomized Dynamic Mode Decomposition for Nonintrusive Reduced Order Modelling." *International Journal for Numerical Methods in Engineering* 112: 3–25.

Brunton, B. W., L. A. Johnson, J. G. Ojemann, and J. N. Kutz. 2016. "Extracting Spatial–Temporal Coherent Patterns in Large-scale Neural Recordings using Dynamic Mode Decomposition." *Journal of Neuroscience Methods* 258: 1–15.

Cacuci, D. G., I. M. Navon, and M. Ionescu–Bujor. 2014. *Computational Methods for Data Evaluation and Assimilation*. Boca Raton: CRC Press.

Cao, L., Z. Chen, P. Jiang, Q. Zhou, and H. Zhou. 2015. "Collaborative Optimization using Hybrid Simulated Annealing Optimization and Sequential Quadratic Programming." Proceedings of the 14th IFToMM World Congress, Taipei, Taiwan, 562–569.

Chen, K. K., J. H. Tu, and C. W. Rowley. 2012. "Variants of Dynamic Mode Decomposition: Boundary Condition, Koopman and Fourier Analyses." *Nonlinear Science* 22: 887–915.

Chopra, A. K. 2000. *Dynamics of Structures*. 4th ed. Prentice-Hall International Series in Civil Engineering and Engineering Mechanics. Harlow: Pearson Education Limited.

Dimitriu, G., R. Stefanescu, and I. M. Navon. 2015. "POD-DEIM Approach on Dimension Reduction of a Multi-species Host-parasitoid System." *Annals of the Academy of Romanian Scientists, Mathematics and its Applications* 7 (1): 173–188.

Du, J., F. Fang, C. C. Pain, I. M. Navon, J. Zhu, and D. Ham. 2013. "POD Reduced Order Unstructured Mesh Modelling Applied to 2D and 3D Fluid Flow." *Computers and Mathematics with Applications* 65: 362–379.

Erichson, N. B., S. L. Brunton, and J. N. Kutz. 2017. "Randomized Dynamic Mode Decomposition." arXiv preprint arXiv:1702.02912.

Erichson, N. B., and C. Donovan. 2016. "Randomized Low-rank Dynamic Mode Decomposition for Motion Detection." *Computer Vision and Image Understanding* 146: 40–50.

Fiedler, M. 2003. "A Note on Companion Matrices." *Linear Algebra and its Applications* 372: 325–331.

Frederich, O., and D. M. Luchtenburg. 2011. "Modal analysis of complex turbulent flow." The 7th International Symposium on Turbulence and Shear Flow Phenomena (TSFP-7), Ottawa, Canada, July 28–31.

Galdi, G. 1994. *An Introduction to the Mathematical Theory of the Navier–Stokes Equation*. New York: Springer-Verlag.

Golub, G. H., and C. F. Van Loan. 1996. *Matrix Computations*. 3rd ed. Baltimore, MD: The Johns Hopkins University Press.

Grammeltvedt, A. 1969. "A Survey of Finite-difference Schemes for the Primitive Equations for a Barotropic Fluid." *Monthly Weather Review* 97 (5): 384–404.

Halko, N., P. G. Martinsson, and J. A. Tropp. 2011. "Finding Structure with Randomness: Probabilistic Algorithms for Constructing Approximate Matrix Decompositions." *SIAM Review* 53 (2): 2017–288.

Jovanovic, M. R., P. J. Schmid, and J. W. Nichols. 2012. "Low-rank and Sparse Dynamic Mode Decomposition." *Center for Turbulence Research Annual Research Briefs*, 139–152.

Koopman, B. 1931. "Hamiltonian Systems and Transformations in Hilbert Space." *Proceedings of the National Academy of Sciences* 17: 315–318.

Krige, D. G. 1951. "A Statistical Approach to Some Mine Valuations and Allied Problems at the Witwatersrand." Master's thesis, University of Witwatersrand.

Kutz, J. N., S. L. Brunton, B. W. Brunton, and J. L. Proctor. 2016. *Dynamic Mode Decomposition: Data-driven Modeling of Complex Systems*. Philadelphia: Society for Industrial and Applied Mathematics.

Kutz, J. N., X. Fu, and S. L. Brunton. 2016. "Multi-resolution Dynamic Mode Decomposition." *SIAM Journal of Applied Dynamical Systems* 15: 713–735.

Kutz, J. N., X. Fu, S. L. Brunton, and N. B. Erichson 2015. "Multi-resolution Dynamic Mode Decomposition for Foreground/background Separation and Object Tracking." IEEE International Conference on Computer Vision Workshop, 921–929.

Mezic, I. 2005. "Spectral Properties of Dynamical Systems, Model Reduction and Decompositions." *Nonlinear Dynamics* 41 (1–3): 309–325.

Mezic, I. 2013. "Analysis of Fluid Flows via Spectral Properties of the Koopman Operator." *Annual Review of Fluid Mechanics* 45 (1): 357–378.

Muld, T. W., G. Efraimsson, and D. S. Henningson. 2012. "Flow Structures Around a High-speed Train Extracted using Proper Orthogonal Decomposition and Dynamic Mode Decomposition." *Computers and Fluids* 57: 87–97.

Navon, I. M. 1979. "Numerical Methods for the Solution of the Shallow-water Equations in Meteorology." University of the Witwatersrand, Johannesburg (South Africa), ProQuest, UMI Dissertations Publishing, 0533651.

Navon, I. M., F. Brown, and D. H. Robertson. 1990. "Combined Simulated-Annealing and Limited-Memory Quasi-Newton Methods for Determining Structure of Mixed Argon-Xenon Molecular Clusters." *Computers and Chemistry* 14 (4): 305–311.

Navon, I. M., and R. DeVilliers. 1986. "GUSTAF: A Quasi-Newton Nonlinear ADI FORTRAN IV Program for Solving the Shallow-water Equations with Augmented Lagrangians." *Computers and Geosciences* 12: 151–173.

Noack, B. R., M. Morzynski, and G. Tadmor. 2011. *Reduced-order Modelling for Flow Control*. Wien: Springer-Verlag.

Noack, B. R., W. Stankiewicz, M. Morzynski, and P. J. Schmid. 2015. "Recursive Dynamic Mode Decomposition of a Transient Cylinder Wake." Physics Fluid Dynamics, arXiv:1511.06876v1.

Noack, B. R., W. Stankiewicz, M. Morzynski, and P. J. Schmid. 2016. "Recursive Dynamic Mode Decomposition of Transient and Post-transient Wake Flows." *Journal of Fluid Mechanics* 809: 843–872.

Nocedal, J., and S. J. Wright. 2006. *Numerical Optimization*. 2nd ed. New York: Springer-Verlag.

Pendergrass, S. D., J. N. Kutz, and S. L. Brunton. 2016. "Streaming GPU Singular Value and Dynamic Mode Decompositions." arXiv preprint arXiv:1612.07875.

Proctor, J. L., S. L. Brunton, and J. N. Kutz. 2016. "Dynamic Mode Decomposition with Control." *SIAM Journal of Applied Dynamical Systems* 15 (1): 142–161.

Rowley, C. W., I. Mezic, S. Bagheri, P. Schlatter, and D. S. Henningson. 2009. "Spectral Analysis of Nonlinear Flows." *Journal of Fluid Mechanics* 641: 115–127.

Rowley, C. W., I. Mezic, S. Bagheri, P. Schlatter, and D. S. Henningson. 2010. "Reduced-order Models for Flow Control: Balanced Models and Koopman Modes." Seventh IUTAM Symposium on Laminar–Turbulent Transition, Stockholm, Sweden, IUTAM Bookseries, Vol. 18, 43–50.

Saint-Venant, A., and J. C. de Barré. 1871. "Théorie du mouvement non permanent des eaux, avec application aux crues des rivières et a l'introduction de marées dans leurs lits." *Comptes rendus de l'Académie des Sciences* 73: 237–240.

Sayadi, T., P. J. Schmid, and F. Richecoeur. 2015. "Parametrized Data-driven Decomposition for Bifurcation Analysis, with Application to Thermo-acoustically Unstable Systems." *Physics of Fluids* 27: 037102.

Schmid, P. J. 2010. "Dynamic Mode Decomposition of Numerical and Experimental Data." *Journal of Fluid Mechanics* 656: 5–28.

Schmid, P. J., and J. Sesterhenn. 2008. "Dynamic Mode Decomposition of Numerical and Experimental Data." 61st Annual Meeting of the APS Division of Fluid Dynamics, San Antonio, Texas, Vol. 53(15). American Physical Society.

Schmid, P. J., D. Violato, and F. Scarano. 2012. "Decomposition of time-resolved tomographic PIV." *Experiments in Fluids* 52 (6): 1567–1579.

Semeraro, O., G. Bellani, and F. Lundell. 2012. "Analysis of Time-resolved PIV Measurements of a Confined Turbulent Jet using POD and Koopman Modes." *Experiments in Fluids* 53: 1203–1220.

Stefanescu, R., A. Sandu, and I. M. Navon. 2015. "POD/DEIM Reduced-order Strategies for Efficient Four Dimensional Variational Data Assimilation." *Journal of Computational Physics* 295: 569–595.

Tissot, G., L. Cordier, N. Benard, and B. R. Noack. 2014. "Model Reduction using Dynamic Mode Decomposition." *Comptes Rendus Mecanique* 342: 410–416.

Towne, A., O. T. Schmidt, and T. Colonius. 2018. "Spectral Proper Orthogonal Decomposition and its Relationship to Dynamic Mode Decomposition and Resolvent Analysis." *International Journal of Fluid Mechanics* 847: 821–867.

Tu, J. H., C. W. Rowley, D. M. Luchtenburg, S. L. Brunton, and J. N. Kutz. 2014. "On Dynamic Mode Decomposition: Theory and Applications." *Journal of Computational Dynamics* 1 (2): 391–421.

Vreugdenhil, C. B. 1994. *Numerical Methods for Shallow Water Flow*. Dordrecht: Kluwer Academic Publishers.

Wahba, G. 1990. "Spline Models for Observational Data." CBMS-NSF Regional Conference Series in Applied Mathematics. Vol. 59. SIAM.

Williams, M. O., I. G. Kevrekidis, and C. W. Rowley. 2015. "A Data-driven Approximation of the Koopman Operator: Extending Dynamic Mode Decomposition." *Nonlinear Science* 25 (6): 1307–1346.

Xiao, D., F. Fang, C. Pain, and G. Hu. 2015. "Non-intrusive Reduced-order Modelling of the Navier–Stokes Equations based on RBF Interpolation." *International Journal for Numerical Methods in Fluids* 79 (11): 580–595.

Yang, X. S. 2010. *Engineering Optimization: An Introduction with Metaheuristic Applications*. Hoboken: Wiley.